Denoising using Adaptive Thresholding and Higher Order Statistics

Samuel P. Kozaitis and Tim Young
Florida Institute of Technology
Department of Electrical and Computer Engineering
150 W. University Blvd.
Melbourne, FL 32901
kozaitis@fit.edu, tyoung@fit.edu

ABSTRACT

We showed that a hard threshold for wavelet denoising based on higher order statistics is comparable to a second order soft threshold. The hard threshold can be made adaptive by using a third order statistic as an estimate of the noise. In addition, the relationship between an adaptive hard threshold and retaining a fraction of wavelet coefficients is shown. Qualitative and quantitative metrics based on the mean-squared error are used to compare the hard thresholding and a soft-thresholding technique, BayesShrink.

Keywords: correlation, denoising, Gaussian noise, higher-order statistics, thresholding, wavelet transforms

1 INTRODUCTION

Denoising methods based on second-order statistics usually use soft threholding [1]. Denoising methods based on third-order statistics are usually based on hard thresholding because the noise power is not conserved in the third-order domain [2]. In this work, a third-order thresholding method using a global threshold is shown to perform as well as scale-dependent second-order thresholds. The ideal threshold is based on the denoised signal error using both the MSE and MAE metrics.

Two third-order threshold methods were investigated, noise adaptive and coefficient adaptive. The noise adaptive threshold is equal to the product of a constant factor and a noise estimate. The coefficient adaptive threshold assumes that the noise is primarily concentrated within a fixed percentage of small third-order coefficients. This threshold method is defined as the Fraction Coefficients Saved threshold because a fixed percentage of the coefficients are used in signal reconstruction. For this method, the threshold is defined as the amplitude of the smallest coefficient in the set of saved coefficients

The initial threshold optimization and testing was performed using a simulated chirp signal as the reference with additive white Gaussian noise (AWGN). This technique was then extended to other types of signals and various adaptive threshold techniques were investigated.

.

2 HIGHER-ORDER SIGNAL DENOISING

Higher-order statistical denoising is based on the use of third-order correlations to identify wavelet coefficients comprised of mostly signal. We thought of wavelet coefficients as correlation coefficients between a noisy signal and wavelets at different scales and translations. Initially, the second-order cross-correlation *functions* between the

Independent Component Analyses, Wavelets, Neural Networks, Biosystems, and Nanoengineering VII, edited by Harold H. Szu, F. Jack Agee, Proc. of SPIE Vol. 7343, 73430F · © 2009 SPIE · CCC code: 0277-786X/09/$18
doi: 10.1117/12.818719

noisy input signal and each scaled and translated wavelet are calculated and labeled as $b_{jk}(\tau)$. Then the third-order autocorrelation coefficients of $b_{jk}(\tau)$ is calculated. The third-order autocorrelation coefficients of the second-order cross-correlations between wavelets and signal are described as

$$b_{3\,jk}(0,0) = \sum_{\tau=1}^{2m_j-1} \left(b_{jk}(\tau)\right)^3 , \tag{1}$$

where m_j is the length of the wavelet at the *jth* scale, and the summation is performed only over the portion of the signal where the wavelet is supported. The block diagram of our approach is shown in Fig. 1. Because the wavelet coefficients b_{jk} represent single values in each of the functions $b_{jk}(\tau)$, the wavelet coefficients cannot be used to calculate the third-order correlation coefficients. To calculate the function $b_{jk}(\tau)$, the basis functions $w_{jk}(\tau)$ must be available. The third-order correlation coefficients $b_{3jk}(0,0)$ are then thresholded to select which wavelet coefficients are to be used in reconstructing the signal.

The result of the second-order wavelet-signal cross-correlation can be thought as consisting of two parts. One part is the correlation between the input signal and the wavelet, and the second part is the correlation between the noise and the wavelet. The second-order correlation result was written as

$$b_{jk}(\tau) = fb_{jk}(\tau) + nb_{jk}(\tau) , \tag{2}$$

where $fb_{jk}(\tau)$ and $nb_{jk}(\tau)$ represented the noise-free signal-wavelet correlation and the noise-wavelet correlation respectively. Substituting Eq. (2) into Eq. (1) and rearranging, the expression for the third-order autocorrelation coefficient can be written as [3,4],

$$b_{3\,jk}(0,0) = \sum_{\tau=1}^{2m_j-1} \left(fb_{jk}(\tau)\right)^3 + 3\sum_{\tau=1}^{2m_j-1} \left(fb_{jk}(\tau)\right)^2 nb_{jk}(\tau) + 3\sum_{\tau=1}^{2m_j-1} fb_{jk}(\tau)\left(nb_{jk}(\tau)\right)^2 + \sum_{\tau=1}^{2m_j-1} \left(nb_{jk}(\tau)\right)^3 . \tag{3}$$

If we assume zero-mean noise, the second term in Eq. (3) will statistically approach zero as the length of the signal increases. If the noise has a symmetric distribution, then the last term will also approach zero. The third term is related to the product of the signal and the noise power. It can be minimized if the mean of the signal is set to zero over the region of correlation. The first term, the third-order correlation, is not due to noise and can be separated from the remaining terms using a threshold.

3 RESULTS

We showed a method for obtaining a consistent measure of noise power using the third order coefficients for the two different signal types shown in Fig. 2. In all experiments, the input signals had lengths of 256 samples and used four levels of the wavelet transform using the Symmlet8 wavelet. Figure 3 is a comparison of the noise estimates in the

second- and third-order domains as a function of input noise level for the reference signals in Fig. 2. In both domains, the noise estimates are consistent for both types of signals.

We used the noise estimate in the development of two fundamentally different third-order threshold algorithms. The noise adaptive threshold method adapts to the noise in the signal by using a threshold that is the product of a constant defined by a factor of *K* and the noise estimate in the third-order domain. Another threshold method was based on maintaining a constant False Declaration Rate (FDR). For this method, the threshold was implemented by reconstructing the signal using a fixed number of coefficients.

For both algorithms, the parameters were optimized using an oracle algorithm. The purpose of the oracle was to obtain the threshold that provided the best third-order algorithm performance. The oracle uses the reference signal to determine the ideal threshold by minimizing the mean squared error (MSE) between the reconstructed and reference signals. The ideal threshold was compared to the noise adaptive threshold using a *K*-factor of 3. The graphs of these thresholds for the chirp and spires signals are in Figs. 4(a) and 4(b) respectively. The ideal and noise adaptive thresholds both exhibit similar trends relative to the input noise level. Fig. 5 shows graphs of the ideal threshold and the noise adaptive threshold with a *K*-factor of 5.

Figures 6 and 7 show graphs of the ideal and FDR thresholds retaining 10 and 30 percent of the wavelet coefficients respectively. Over the range of input noise levels, the FDR threshold for 10 percent tends to track the ideal threshold better than the noise adaptive threshold with a *K*-factor of 5.

We defined a threshold error as the absolute difference between the ideal threshold and one computed by a particular algorithm. Fig. 8 shows histograms of threshold errors for an SNR of 1 using the signal of Fig. 2(a). The histogram represents 1000 signal instances. Figs. 8(a) and 8(b) are for the FDR of 10 and 30 percent respectively. Figs. 8(c) and 8(d) show the results for the noise adaptive threshold with *K*-factors of 3 and 5 respectively. The ideal threshold algorithm would have an error histogram centered at zero. Therefore we seek an algorithm that provides the maximum number of zeros in the histogram. Both the FDR at 10 percent and the noise adaptive threshold with a *K*-factor of 5 are nearly identical in terms of the number of near zero errors.

We compared the third-order denoising algorithm to the 1-D version of the BayesShrink algorithm[5]. The third-order results are shown in Fig. 9 and the BayesShrink results are in Fig. 10. Fig. 9 shows the reference signal, noisy input, and reconstructed signal from Fig. 2(a) for the noise adaptive threshold with a *K*-factor of 5 and SNR = 1. Using the MSE as the only measure of performance the BayesShrink performs better than the third-order method. However, the MSE does not accurately measure how well the algorithms preserve features of the signal. For example, the higher frequencies of the chirp are suppressed by the BayesShrink but preserved by the third-order method.

The performance using the spires signal is shown in Fig. 11 for the noise adaptive algorithm and Fig. 12 for the BayesShrink algorithm. The *K*-factor is 5 and the SNR is 0.87. The spires signal has very noticeable peaks or features that are maintained by the third-order algorithm better than BayesShrink algorithm. Once again it can be seen that the MSE does not accurately measure the ability of the third-order to maintain specific details of the signal.

Figure 13 shows graphs of the MSE vs noise level for the oracle and noise adaptive threshold with a *K*-factor of 5. For both signals types in Fig. 2 the oracle performs better. Figure 14 shows graphs of MSE vs noise level for the oracle and BayesShrink algorithm. For both signal types in Fig. 2 the oracle performs better at the higher noise levels. At lower noise levels, BayesShrink performs better for the signal in Fig. 2(a), and both methods' performance converge for the signal in Fig. 2(b).

4 CONCLUSION

We found that the ideal threshold and the third-order noise estimate behave similarly relative to the input noise level enabling the noise adaptive threshold algorithm to provide good performance in terms of MSE. It was also shown that the performance of the third-order is robust to variations in the exact value of the threshold based on the MSE.

Alternatively, we found that although the FDR threshold more closely matches the ideal threshold, the noise adaptive threshold performs better. Based on using the MSE metric the performance of the third-order can be improved by improving the threshold estimation method.

REFERENCES

[1] F. Luisier, T. Blu, and M. Unser, "A new SURE approach to image denosing: interscale orthonormal wavelet thresholding," *IEEE Trans. on Image Processing,*. 16(3), 593-606 (2007).

[2] S. P. Kozaitis, "Improved feature detection in ECG signals through denoising," *Int*. *Journal of Signal and Imaging Systems Engineering,* 1(2), 108-114 (2008).

[3] J. M. Mendel, "Tutorial on higher-order statistics (spectra) in signal processing and system theory: theoretical results and some applications," *Proc. IEEE* 79(3), 278-305, (1991).

[4] G. B. Giannakis, and M. K. Tsatsanis, *IEEE Trans. on Acoustics, Speech, and Signal Processing*, 38, 1284-1296 (1990).

[5] S. G. Chang, B. Yu, M. Vetterli, "Adaptive Wavelet Thresholding for Image Denoising and Compression*", IEEE Trans. Image Processing*, 9, pp 1532-1546, Sep. 2000.

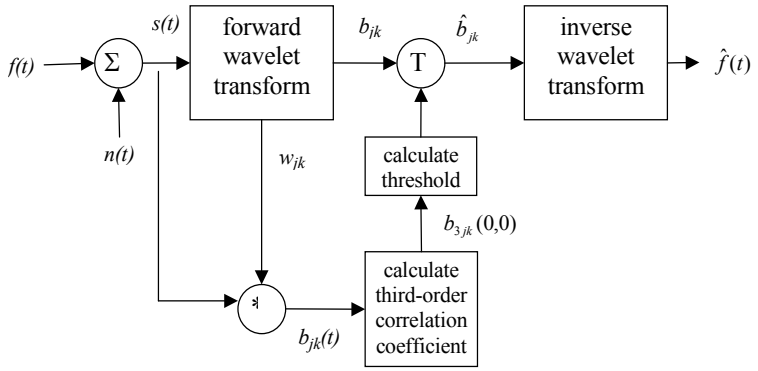

Figure 1 Third-order denoising approach.

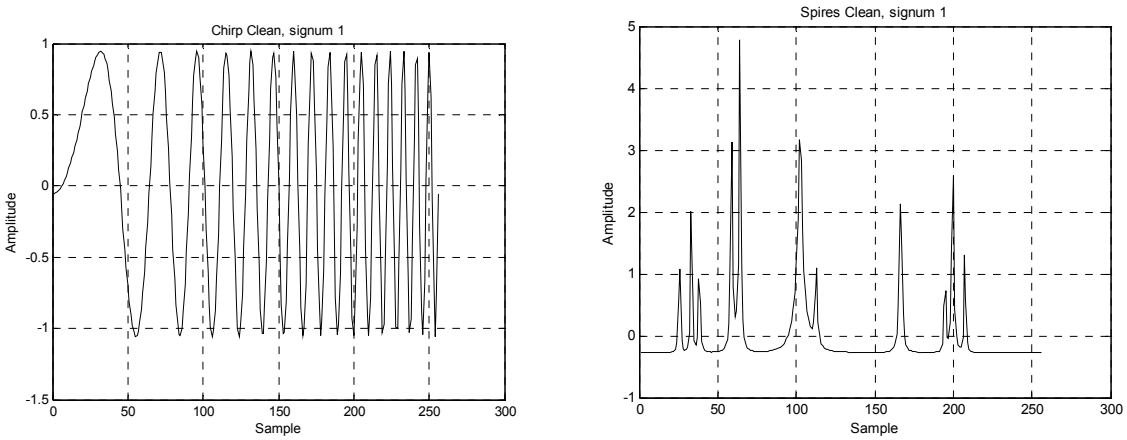

Figure 2 Reference signals used in experiments (a) chirp (b) spires.

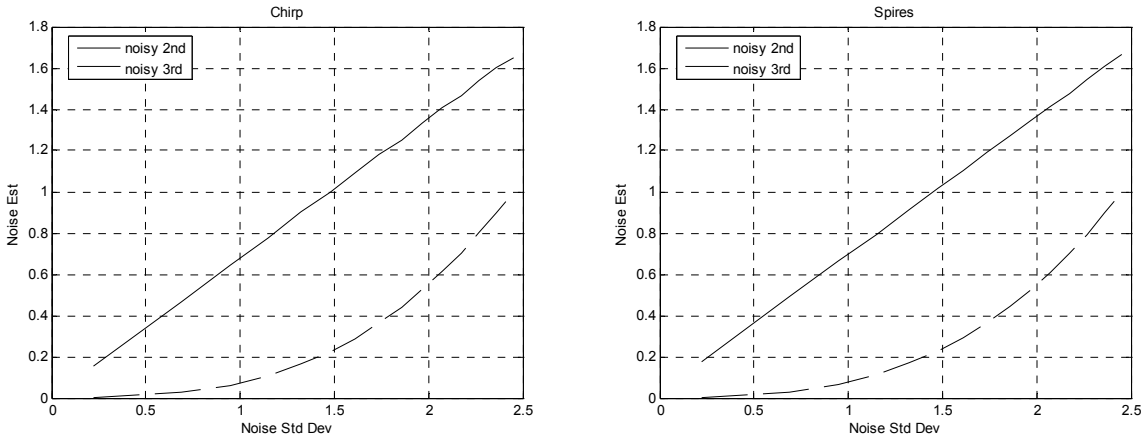

(a) (b)

Figure 3 Noise estimate as a function of input noise standard deviation in both second- and third-order domains for reference signals (a) signal in Fig 2a (b) signal in Fig 2b. Each point in the graph represents an average of 1000 trials.

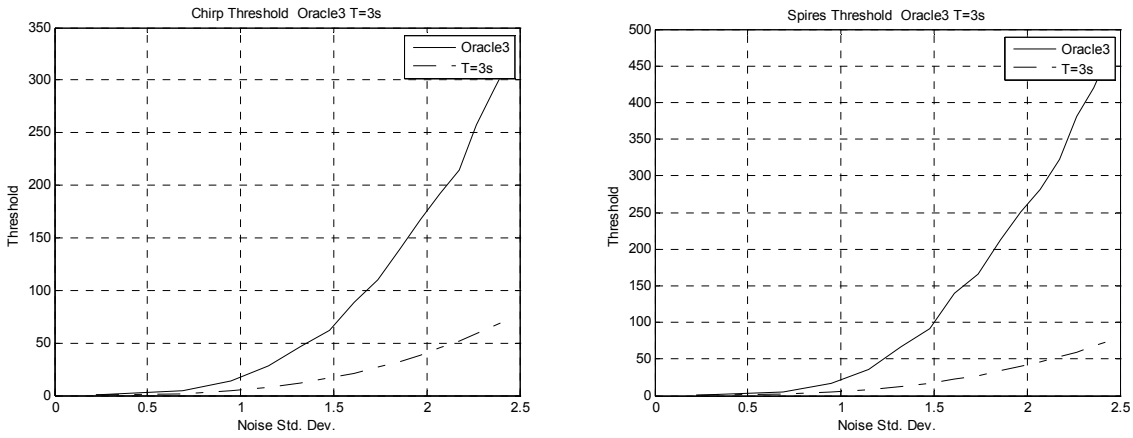

(a) (b)

Figure 4 Threshold comparison of ideal and adaptive threshold for *K*-factor = 3 (a) signal in Fig. 2a (b) signal in Fig. 2b. Each point in the graph represents an average of 1000 trials.

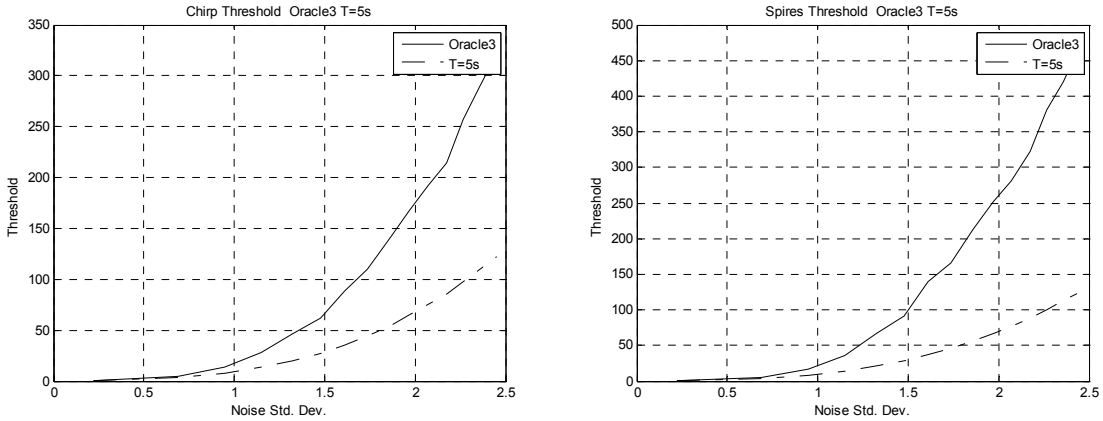

(a) (b)

Figure 5 Threshold comparison of ideal and adaptive threshold for *K*-factor = 5 (a) signal in Fig. 2a (b) signal in Fig. 2b.

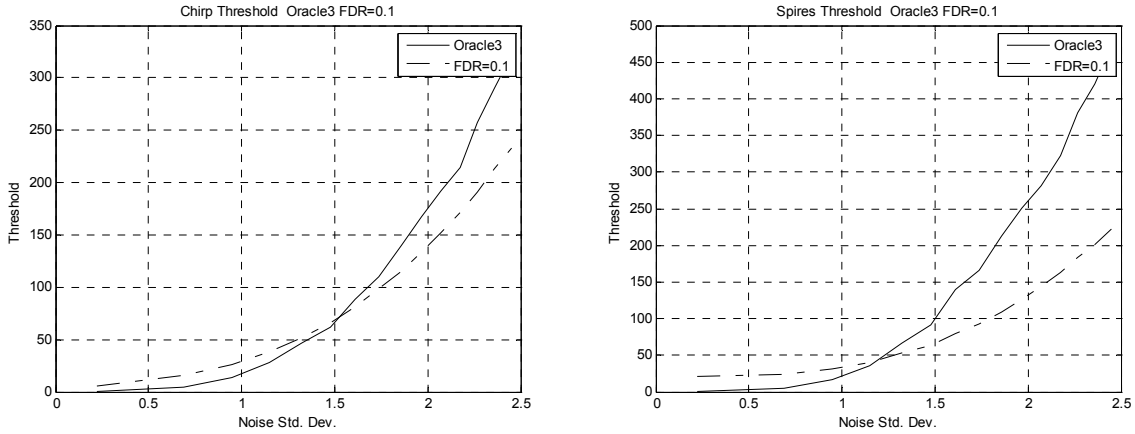

(a) (b)

Figure 6 Threshold comparison of ideal and FDR method using 10 percent of the wavelets coefficients (a) signal in Fig. 2a (b) signal in Fig. 2b.

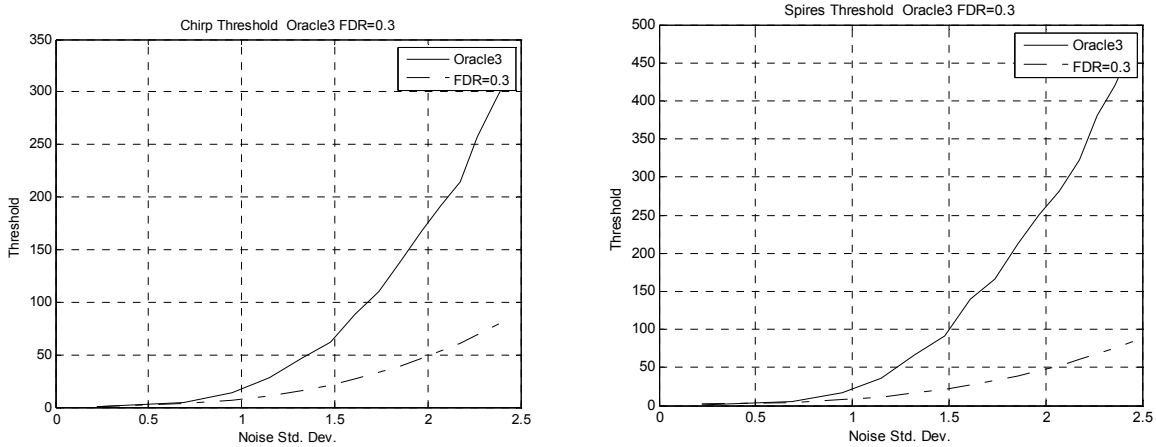

(a) (b)

Figure 7 Threshold comparison of ideal and FDR method using 30 percent of the wavelets coefficients (a) signal in Fig. 2a (b) signal in Fig. 2b.

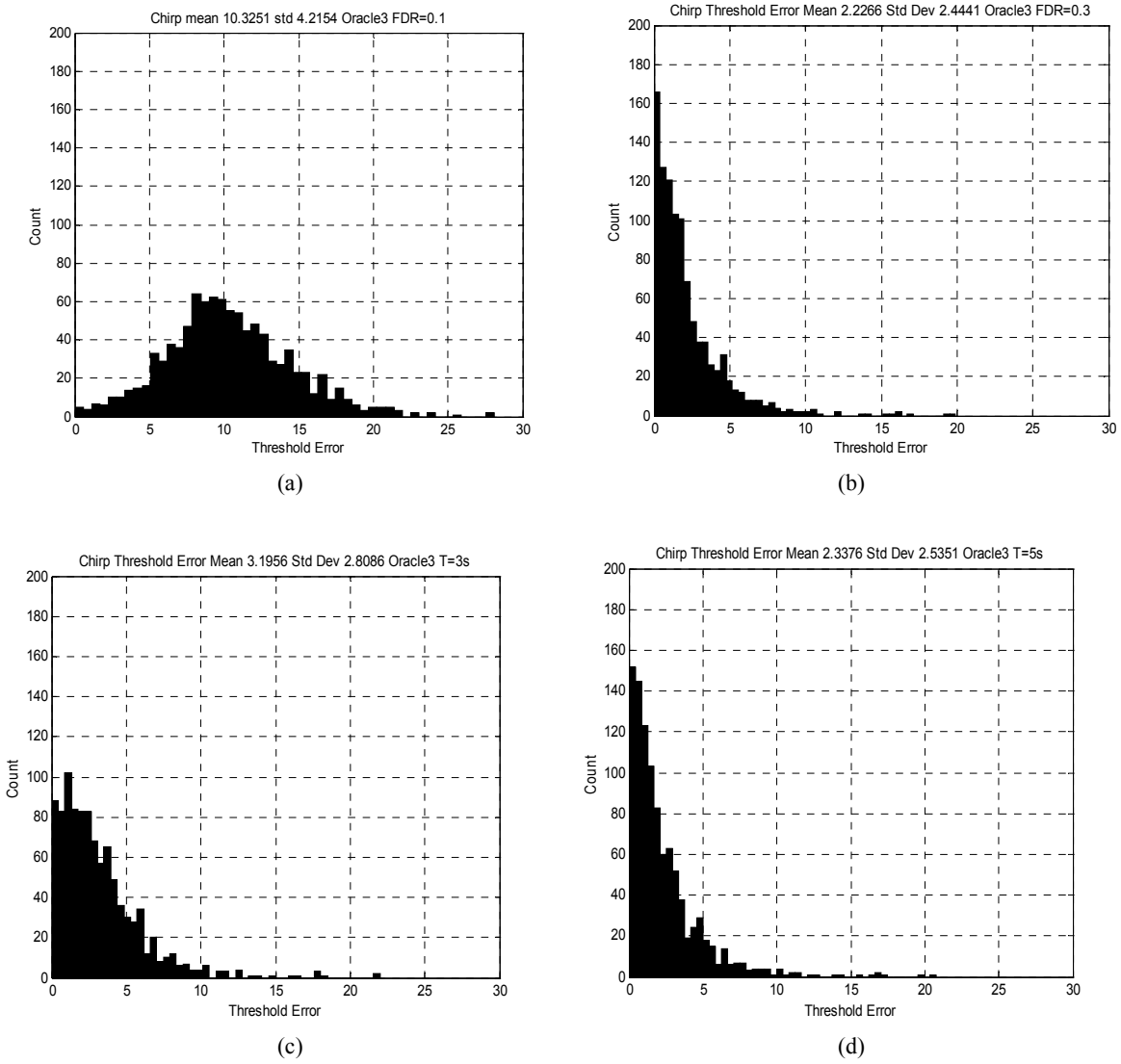

Figure 8 Threshold difference histograms using the signal in Fig. 2a for ideal and 3rd order thresholds (a) FDR for 10 percent (b) FDR for 30 percent (c) *K*-factor = 3 (d) *K*-factor 5.

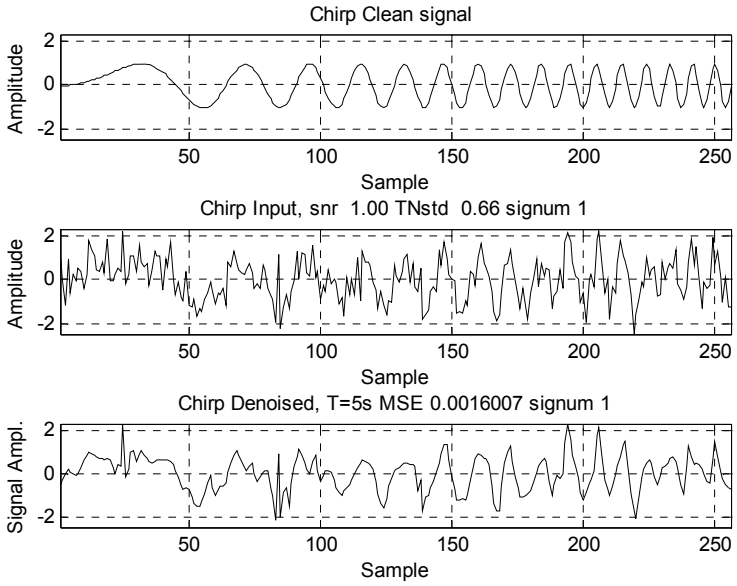

Figure 9 Third-order algorithm used on signal in Fig. 2a using noise adaptive *K*-factor of 5.

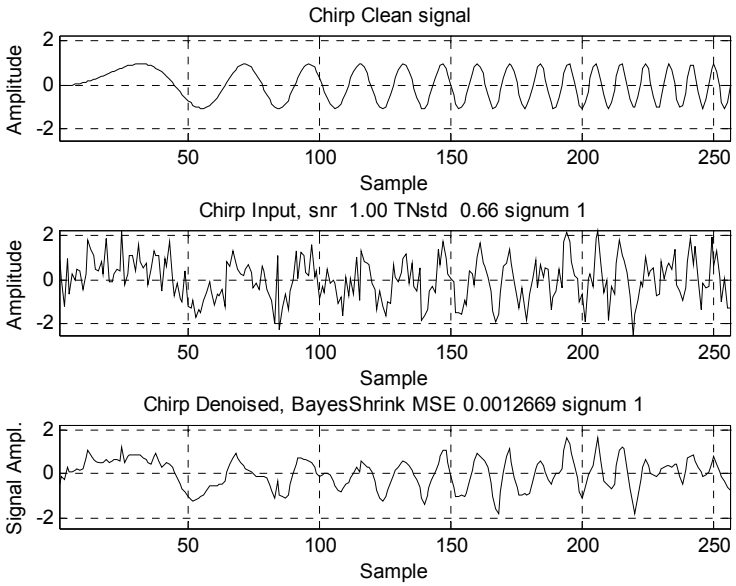

Figure 10 BayesShrink algorithm used on signal in Fig. 2a.

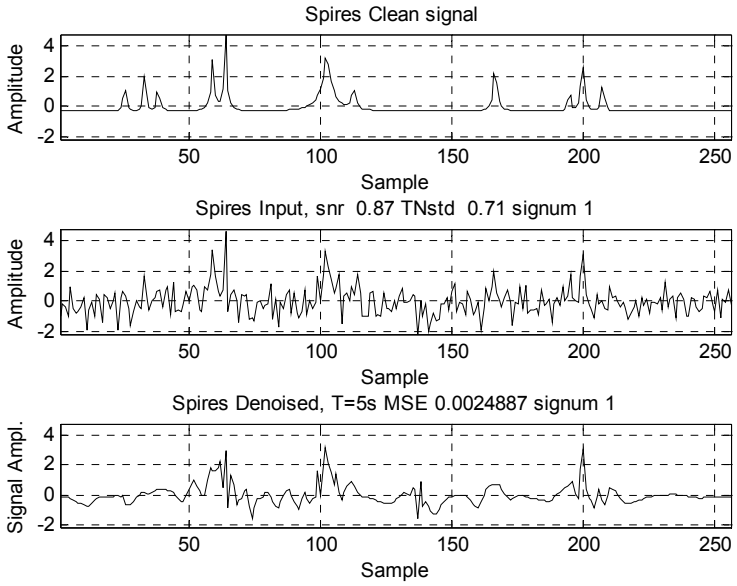

Figure 11 Third-order algorithm used on signal in Fig. 2b using noise adaptive *K*-factor of 5.

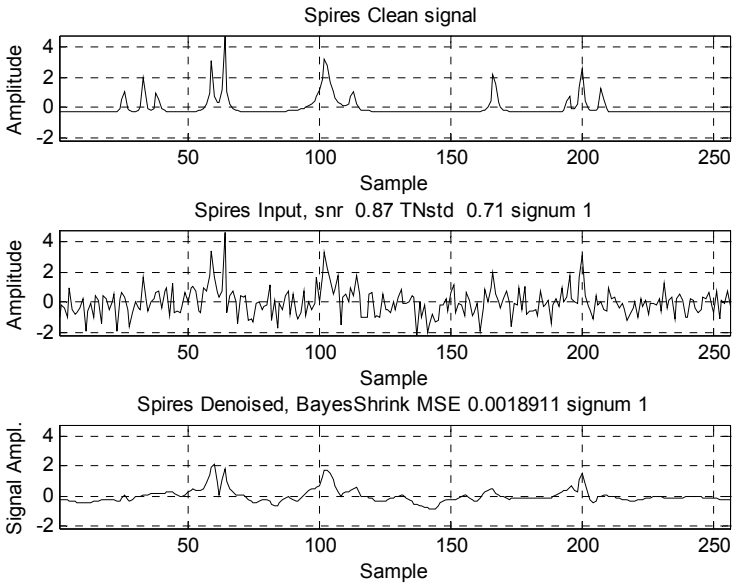

Figure 12 BayesShrink algorithm used on signal in Fig. 2b.

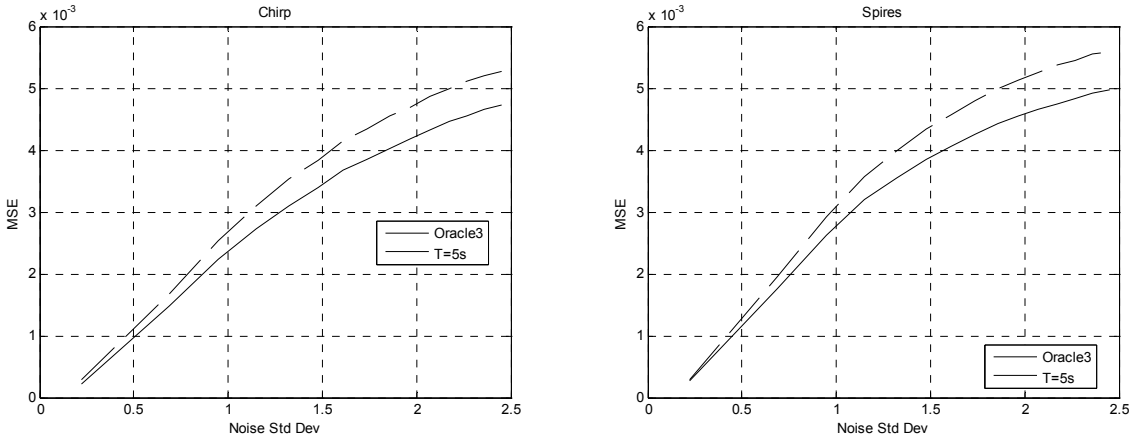

Figure 13 Performance comparisons of oracle and adaptive *K*-factor = 5 using MSE Metric (a) signal in Fig. 2a (b) signal in Fig. 2b.

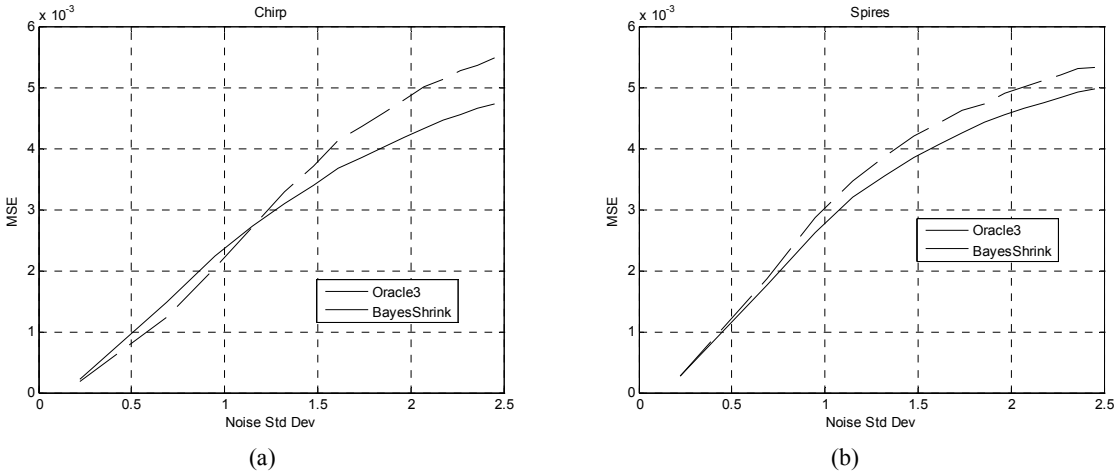

Figure 14 Performance comparisons of oracle and BayesShrink using MSE Metric (a) signal in Fig. 2a (b) signal in Fig. 2b.